View metadata, citation and similar papers at core.ac.uk
brought to you by CORE
provided by CERN Document Server

arXiv:astro-ph/0007002 v1 1 Jul 2000

Stellar Populations in the Host Galaxies of Mrk 1014, IRAS 07598+6508, and Mrk 231[1]

Gabriela Canalizo[2] and Alan Stockton[2,3]

Institute for Astronomy, University of Hawaii, 2680 Woodlawn Drive, Honolulu, HI 96822

ABSTRACT

We present deep spectroscopic and imaging data of the host galaxies of Mrk 1014, IRAS 07598+6508, and Mrk 231. These objects form part of both the QSO and the ultraluminous infrared galaxy (ULIG) families, and may represent a transition stage in an evolutionary scenario. Our imaging shows that all three objects have highly perturbed hosts with tidal tails and destroyed disks, and appear to be in the final stages of major mergers. The host galaxies of the three objects have spectra typical of E+A galaxies, showing simultaneously features from an old and a young stellar component. We model spectra from different regions of the host galaxies using Bruzual & Charlot (1996) spectral synthesis models using two component models including an old underlying population and recent superposed starbursts. Mrk 1014 has intense star formation concentrated in a large knot < 2 kpc from the nucleus, along the leading edge of the tidal tail, and in several knots scattered around the host. The starburst ages in these regions range from 180 to 290 Myr. IRAS 07598+6508 has multiple knots of star formation concentrated in two regions within 16 kpc of the QSO nucleus, with ages ranging from 30 to 70 Myr; the host galaxy shows an older population in other regions. Mrk 231 shows a wider range of starburst ages, ranging from 42 Myr in the arc 3 kpc south of the nucleus, to ~ 300 Myr spread on a "plateau" ~ 20 kpc across around the nucleus, as well as a UV bright region 12 kpc south of the nucleus, which is apparently a region of currently active star formation. Our results indicate a strong connection between interactions and vigorous bursts of star formation in these objects. We propose that the starburst ages found are indicative of young ages for the QSO activity. The young starburst ages found are also consistent with the intermediate position of these objects in the far infrared color-color diagram.

Subject headings: galaxies: interactions—galaxies: infrared—galaxies: starburst—galaxies: evolution—quasars: individual (Mrk 1014, IRAS 07598+6508, Mrk 231)

---

[1]Based on observations made with the NASA/ESA Hubble Space Telescope, obtained from the data archive at the Space Telescope Science Institute, which is operated by the Association of Universities for Research in Astronomy, Inc., under NASA contract NAS 5-26555.

[2]Visiting Astronomer, W.M. Keck Observatory, jointly operated by the California Institute of Technology and the University of California.

[3]Visiting Fellow, Research School of Astronomy and Astrophysics, Australian National University.

1. Introduction

There has long been considerable circumstantial evidence that at least some luminous, low-redshift QSOs are the result of strong interactions or mergers of galaxies (*e.g.,* Toomre & Toomre 1972; Gunn 1979; Stockton 1982; Hutchings & Neff 1992; McLeod & Rieke 1994; see Stockton 1999 for a review). However, a concrete suggestion for an evolutionary scenario for such objects was lacking until Sanders et al. (1988a) showed that ultraluminous infrared galaxies (ULIGs), virtually all of which are compelling examples of ongoing mergers, had bolometric luminosities and space densities similar to those of QSOs. These similarities suggested the possibility that ULIGs are dust-enshrouded QSOs which, after blowing away the dust, become classical QSOs.

If this hypothesis is correct, one should be able to observe examples of objects that are at intermediate stages of this evolutionary sequence. We are conducting a study of a sample of low-redshift objects that may be in such a transitionary state. These objects are recognized as bona-fide QSOs and are found at an intermediate position in a far infrared (FIR) color-color diagram between the regions occupied by typical QSOs and ULIGs (see Fig. 1). FIR color–color diagrams have been used as tools to detect and discriminate different types of activity in the nuclear and circumnuclear regions of galaxies. Different kinds of objects such as QSO/Seyfert, starbursts, and powerful IR galaxies, occupy fairly well defined regions in the diagram (see, *e.g.,* Neugebauer et al. 1985; de Grijp et al. 1987; Taniguchi et al. 1988; Lípari 1994). With deep imaging and spectroscopic observations of the host galaxies, we are attempting to construct interaction histories for each of these "transition" objects.

If strong interactions triggered the QSO activity and induced starbursts, one might expect both events to occur roughly simultaneously, since both are plausibly dependent on gas flows to the inner regions. Thus, we are placing these objects on an age sequence by measuring the time elapsed since the last major starburst event. This age sequence along with interaction histories can help us answer the question of whether the intermediate position of these objects is indicative of evolution from the ULIG to the classical QSO population, or whether it simply indicates a range of characteristics in QSOs.

Our sample is drawn from the Neugebauer et al. (1986), Low et al. (1988), and Clements (1996) samples of *Infrared Astronomical Satellite*[2] (*IRAS*) objects, and it consists of those objects which have: (1) a luminosity above the cutoff defined for quasars by Schmidt & Green (1983), *i.e.,* $M_{\rm B} = -23$ for $H_0 = 50$ km s^{-1} Mpc^{-1} (or $M_{\rm B} = -22.1$ for $H_0 = 75$ km s^{-1} Mpc^{-1}), (2) a redshift $z \leq 0.4$, (3) a declination $\delta \geq -30°$, (4) firm *IRAS* detections at 25μm, 60μm, and 100μm, and (5) a position in the FIR color–color diagram which is intermediate between the ULIG and QSO loci (Fig. 1). Although Mrk 231 just misses the luminosity threshold given above, its active nucleus is known to suffer heavy extinction (see §5), apart from which it would clearly be a member of the sample. We know of no other objects satisfying the other criteria for which this is true. We have therefore chosen to include it for the present, although it may be approriate to exclude it from

some of the analyses of the whole sample, which will be presented in a subsequent paper.

So far, we have presented results for two of the nine objects in the sample: 3C 48 (Canalizo & Stockton 2000, hereafter CS2000), an ongoing merger near the peak of starburst activity; and PG 1700+518 (Canalizo & Stockton 1997; Stockton et al. 1998, hereafter CS97 and SCC98; see also Hines et al. 1999), where a tidally disturbed companion with a dominant 85 Myr old post-starburst population may be in the process of merging with the host galaxy. In this paper we present the results for three additional objects: Mrk 1014, IRAS 07598+651, and Mrk 231. We assume $H_0 = 75$ km s^{-1} Mpc^{-1} and $q_0 = 0.5$ throughout this paper, so that the projected physical length subtended by $1''$ is 2.43 kpc for Mrk 1014, 2.26 kpc for IRAS 07598+651, and 0.77 kpc for Mrk 231.

2. Observations and Data Reduction

Spectroscopic observations for the three objects were carried out using the Low-Resolution Imaging Spectrometer (LRIS; Oke et al. 1995) on the Keck II telescope. For IRAS 07598+6508, we used a 600 groove mm^{-1} grating blazed at 5000 Å yielding a dispersion of 1.28 Å pixel^{-1}. For Mrk 231 and Mrk 1014, we used a 300 groove mm^{-1} grating blazed at 5000 Å with a dispersion of 2.44 Å pixel^{-1}. The slit was $1''$ wide, projecting to ∼5 pixels on the Tektronix 2048×2048 CCD. We obtained two or three exposures for each slit position, dithering along the slit between exposures. Table 1 shows a complete journal of observations, with specification of the slit positions, and total integration times.

The spectra were reduced with IRAF, using standard reduction procedures. After subtracting bias, dividing by a normalized halogen lamp flat-field frame and removing sky lines, we rectified the two-dimensional spectra and placed them on a wavelength scale using the least-mean-squares fit of cubic spline segments to identified lines in a Hg-Kr-Ne lamp. We calibrated the spectra using spectrophotometric standards from Massey et al. (1988) observed with the slit at the parallactic angle. The distortions in the spatial coordinate were removed with the IRAF *apextract* routines. For each slit position, we had two or three individual frames; we averaged the spatially corrected spectra using the IRAF task *scombine*. We then corrected the spectra for Galactic extinction, using the values given by Schlegel et al. (1998).

Since we were aiming to observe the youngest populations in the host galaxies of these objects, we chose the slit positions based on previously obtained color maps of the host galaxies. We obtained imaging data for the three objects with the University of Hawaii 2.2 m telescope as specified in Table 2. Observations with the U' filter (centered at 3410 Å with a bandpass of 320 Å) sample the spectral energy distribution (SED) of galaxies on the short side of both the 4000 Å break and the

[1]The Infrared Astronomical Satellite was developed and operated by the US National Aeronautics and Space Administration (NASA), the Netherlands Agency for Aerospace Programs (NIVR), and the UK Science and Engineering Research Council (SERC).

Balmer limit. This region is very sensitive to the age of the stellar population, and will be brightest in regions of very recent star formation (ages $\lesssim 100$ Myr), as well as regions with scattered QSO continuum. Observations in $B-$band sample the region redwards of the Balmer limit, where $\sim$A-type stellar populations are expected to peak, while longer wavelength optical and near infrared images will map the distribution of late-type stellar populations. The $U'-B$ color maps will then highlight the regions of most recent star formation while $B-R'$ will point to the somewhat older ($\gtrsim 200$ Myr) populations. Thus our slit positions generally cover the regions brightest in these color maps. In general, the spectra from each slit position were subdivided into regions corresponding to some of the main features observed in the optical ground-based images, and one-dimensional spectra were extracted by summing pixels corresponding to the regions of interest.

The spectra of regions close to the QSO nucleus were contaminated by scattered QSO light. The scattered light was removed by subtracting from each region a version of the quasar nuclear spectrum, scaled to match the broad-line flux. In the case of Mrk 1014, none of our slit positions went through the QSO, so we obtained a separate 200 s exposure of the nucleus.

Spectra from those slit positions which actually went through the QSO nucleus suffered from strong light scattering within the spectrograph, particularly in the spectral region around Hα. Therefore we were unable to obtain spectra of regions closer than $\sim 2''$ from the QSO nucleus for these slit positions.

HST WFPC2 images of the three objects were obtained from the *HST* data archive. We used three 600 s WFC2 images of Mrk 1014 in the F675W filter, one 400 s and two 600 s PC1 images of IRAS 07598+6508 in the F702W filter, and two 1100 s PC1 images of Mrk 231 in the F439W filter. Most cosmic rays were removed by subtracting a median image from each of the individual frames, then thresholding the difference at a 3σ level, setting points above this threshold to the median of the difference image. Pixels near the position of the peak of the QSO were excluded from this process. The corrected difference image was then added back to the median image, giving a corrected version of the original image. The few cosmic rays within the relevant region that escaped this process were removed manually with the IRAF task *imedit*. In the case of Mrk 231, where only two images were available, we first subtracted one from the other, and proceeded as above. The procedure was repeated, interchanging the images. All the corrected images for each object were then averaged.

2.1. Modeling Spectra

We use Bruzual & Charlot (1996) isochrone synthesis models to fit the spectra of the host galaxies. We will see in the following sections that the three objects which are the subject of this paper show strong evidence of having undergone some major tidal interaction. As we have described in our previous work (CS97, CS2000), spectra of the host galaxies of such objects show features from both young (*e.g.,* strong Balmer lines) and old (*e.g.,* Mg I *b* absorption) stellar populations, and can

usually be fitted satisfactorily by a two-component model. This model includes an old underlying stellar population, presumably the stellar component present prior to interaction, and a younger instantaneous burst model, presumably produced as a result of the interaction. A population with no age dispersion will be a reasonable approximation of the actual starburst as long as the period during which the star formation rate was greatly enhanced is short compared to the age of the population itself.

We have also noted previously (SCC98) that the age of the superposed starburst is remarkably robust with respect to the different assumptions about the nature of the older stellar component. Thus, we select a reasonable old underlying population (with certain variations as described in each section below) and assume that the same underlying population is present everywhere in the host galaxy. To this population we add instantaneous burst, Scalo (1986) initial mass function, solar metallicity models of various ages. We then perform a χ^2 fit to the data to determine the scaling of each component and the age of the most recent starburst. The errors in the starburst ages that we quote are estimated by noting the youngest and oldest best fits for which χ^2 changes by 15% with respect to the minimum value (see CS2000 for details).

In some cases, stellar absorption features (most often the Balmer lines) were contaminated by emission coming from the extended narrow emission line region around the QSO. In some cases, we subtracted a scaled synthetic spectrum of the recombination lines assuming Case B. However, in calculating χ^2 for the model fitting, we generally excluded those lines that suffered most from contamination. All spectra are displayed as observed (*i.e.,* without line subtraction), unless otherwise specified.

As we discussed in CS2000, because of our limited spatial resolution (generally $1'' \times 1''$) and projection along the line of sight, we are likely observing the integrated spectrum of several starbursts of different ages, and the age we determine will be somewhat older than the youngest starbursts. Therefore the ages we report should be regarded as upper limits to the most recent episodes of star formation along the line of sight.

In objects with recent starbursts, the effect of reddening by dust is an obvious concern. However, studies of low-redshift AGNs and ULIGs at millimeter and submillimeter wavelengths indicate that dust is generally heavily concentrated within $\sim$ 1 kpc of the nucleus (Andreani et al. 1999; Bryant & Scoville 1996). In addition, have found (SCC98) that even in a case where the optical—IR spectral index is strongly affected by dust, the stellar ages from spectral features in the rest-frame 3200–5200 Å region remain fairly robust. This relative insensitivity to dust can be attributed to the fact that we are largely dealing with dust that is intermixed with the stars and that we preferentially observe regions with low extinction and, thus, low reddening. Even in regions where dust along the line of sight is significant, the reddening in our observed bandpass is likely to be largely compensated by blue light scattered into our line of sight.

3. Mrk 1014

Mrk 1014 ($z = 0.163$) is a luminous ($M_B = -23.9$), infrared loud (*e.g.,* Sanders et al. 1988b) radio-quiet QSO which shows a luminous host galaxy. The host galaxy has two large "spiral-like arms" (MacKenty & Stockton 1984; see Fig. 2 and Fig. 3). Its spectrum indicates a mixture of old and young stars (MacKenty & Stockton 1984; Heckman et al. 1984; Hutchings & Crampton 1990).

Recently, Nolan et al. (2000), in a spectroscopic survey of 26 RLQs, RQQs, and radio galaxies, observed the host galaxy of Mrk 1014 with the Mayall 4 m telescope at Kitt Peak National Observatory and with the 4.2 m William Herschel telescope at La Palma. They modeled the spectra and determined an age of 12 Gyr for the host galaxy of Mrk 1014. Their approach is exactly opposite to ours (see §2.1): they fix the age of a possible young single starburst population to 0.1 Gyr and let that of a second, older single starburst population (what we would call the "underlying population") vary. Their reason for including the 0.1 Gyr population is to account for "the spectral shape of the blue light" which they attribute to either a recent burst of star formation or contamination of the slit by scattered light from the QSO nucleus. Their results will be discussed further in §3.1.

3.1. Stellar Populations

The host galaxy of Mrk 1014 shows stellar absorption features with redshifts remarkably close to those of the QSO broad and narrow emission lines ($z_{\rm QSO} = 0.1634$, as measured from our spectrum).

We have obtained and modeled spectra of different regions in the host galaxy of Mrk 1014, and we shall refer to them according to their label in Fig. 4. We have chosen a 10 Gyr old population with an exponentially declining star formation rate with an e-folding time of 3 Gyr as an old underlying population. This model fits reasonably well the spectrum of a galaxy $60''$ west-southwest of the QSO at the same redshift and only slightly smaller than the "bulge" (see below) of Mrk 1014. (This galaxy was in our slit while obtaining the 200 s exposure of the QSO). The assumption that the host galaxy (or parent galaxies) of Mrk 1014 had a similar star formation history to this galaxy need not be accurate as the precise model we use as the pre-existing population makes little difference in the age determination of the starburst population (SCC98). For comparison, we have tried using a generic elliptical galaxy spectrum, and a model with a longer e-folding time (*i.e.,* 5 Gyr) as underlying populations in the modeling of the spectra in Mrk 1014. We obtain the same starburst ages, though slightly different flux contributions from the old population, regardless of the model used.

Figure 2 includes a $B' - R'$ color map of Mrk 1014. This image emphasizes those regions with a steeper blue continuum spectrum, peaking just redwards of the Balmer limit. These regions are concentrated mainly along the north edge of the tail (regions *a* and *b* in Fig. 4), in a clump on the east end of the tail (*c*), directly east of the nucleus (not covered by our slits), and southwest of the

QSO nucleus (e).

Spectroscopy of these regions confirms that they are indeed the youngest stellar populations we find in the host, with ages ranging from 180 Myr in region e to 290 Myr in region d. Figure 5 shows the spectrum of region a, with the best χ^2 fit of the model to the data superposed, and the relative contributions of the 200 Myr starburst and the old underlying population. The error in these ages is typically ± 50 Myr. Figure 3 shows compact knots at the positions of regions a through d, and Planetary Camera *HST* images (Surace et al. 1998) show a larger and very bright blue knot at the position of region e. Even though there are knots at the positions of a and b, it is evident from colors and spectroscopy that there is recent star formation all along the north edge of the tail (*i.e.,* between a and b).

Other regions of the host galaxy appear redder in the $B' - R'$ color map in Fig. 2. These regions, sampled by f and g, appear to be dominated by an older, ~ 1 Gyr population, and to have very little, if any, contribution from the old underlying population (Fig. 6, top panel). It is not entirely clear whether these are truly intermediate age populations, or if they are simply, as in the case of region h, dominated by an old underlying population with a very small contribution from a younger population like those found in regions a through e. We attempted to fit models with the latter characteristics to the observed spectra. The resulting fits are reasonable, with minimum values of χ^2 10% and 25% larger than that obtained for a dominant intermediate-age population for regions f and g respectively. The bottom panel of Fig. 6 shows the spectrum of region f with the best fit to the data of the sum of an old underlying population and a 250 Myr instantaneous burst population. While a reasonable fit, it does show significant discrepancies in the region around the 4000 Å break and the Ca II K line.

The potential presence of this intermediate age population suggests that a better fit for the younger populations might be achieved by adding a third component that accounts for this intermediate age component. However the flux of the young starburst population in those regions is so dominant (typically contributing 80% of the total flux at rest-frame 5000 Å), that a third component makes a negligible difference to the fit.

Region i shows very strong emission, which almost certainly comes from gas ionized by the QSO rather than from star-forming regions. The equivalent widths of the emission lines here are greater than those of the emission lines elsewhere in the galaxy by at least a factor of 5, and at least twice those of the QSO nucleus for [O III]. The emission line ratios indicate a power-law ionizing continuum (Veilleux & Osterbrock 1987). This region is clearly seen as a large, discrete knot in Fig. 2*d* of Stockton & MacKenty (1987). The gas has an approaching velocity of 180 ± 50 km s^{-1} with respect to the stellar absorptions in that region. The underlying spectrum is similar to that of region h.

Region h also shows emission lines with approaching velocities of ~ 200 km s^{-1} with respect to the stellar features, but this region shows an additional, weaker emission component clearly visible in [O II], [O III], and Hβ, blueshifted by 1150 ± 50 km s^{-1} with respect to the stronger component.

The stellar population here seems to be dominated by an old population with a small fraction of the flux coming from younger stars.

We have added spectra from two different slit positions at region j to improve the signal to noise in this very faint region. This is part of the long extension on the west side clearly seen in the high contrast image in Fig. 2. We find a continuum with a red SED and a clear 4000 Å break at a redshift close to, but slightly larger than that of the main body of the galaxy.

Region k, which is very bright in the R' image in Fig. 2, would appear to be an extension of the east tail. However, its spectrum shows that it is a background galaxy at $z = 0.5843$. Likewise, region l on the west tail is a galaxy at $z = 0.5857$. A third galaxy SE of the QSO ($\Delta\alpha = +11\farcs9$, $\Delta\delta = -40''$) has a similar redshift as well ($z = 0.5838$), so there seems to be a group or cluster of galaxies at this redshift.

The 200 s exposure spectrum of the elongated object $9\farcs2$ west-southwest of the QSO shows narrow emission lines at the same redshift as the QSO superposed on a red continuum. Fig. 2*d* of Stockton & MacKenty (1987) shows that there is strong emission just north of this object coming from extended gas ionized by the QSO and not necessarily associated with the object. The spectrum is too noisy to distinguish stellar features, so it is unclear whether this object is interacting with the system or if it is a chance projection. The near edge-on galaxy $\sim 23''$ west of the QSO, on the other hand, shows [O III] emission confined to the galaxy at $z = 0.162$ in a University of Hawaii 2.2 m telescope spectrum (Canalizo 2000, unpublished), as suggested by Stockton & MacKenty (1987) from their [O III] imaging.

How do our results compare to those of Nolan et al. (2000)? As mentioned above, Nolan et al. use a fixed 0.1 Gyr starburst population. They determine that this population makes up 1.1% of the total luminous mass along the line of sight, and that the rest of the flux is well characterized by a 12 Gyr instantaneous burst. In contrast, we find several regions of recent ($\sim$ 0.2 Gyr) star formation where the star forming mass typically amounts to 12%, and sometimes up to 30%, of the total luminous mass along the line of sight. One of our slit positions is very similar to one used by Nolan et al. (see Fig. 2 in Hughes et al. 2000), but our slit is narrower and slightly closer to the nucleus. As a way to compare, we added the flux along the slit as Nolan et al. seem to have done, including the background galaxy k, which is also in their slit. Even if we add up all the flux along this slit (subtracting the QSO light, which amounted to 5% of the total flux), we still find that the star forming regions make up 8% of the total luminous mass along the line of sight. Obviously, the difference in ages will lead to a smaller percentage for their choice of parameters. So, we tried fixing our parameters to match theirs (*i.e.,* 12 Gyr + 0.1 Gyr populations), and this yields a 5% by mass for the young population, but the fit is much inferior to the ones discussed in this section. Their slit position may have fortuitously missed the major star forming regions, thus leading to this smaller percentage. We have previously cautioned (CS2000) that different slit positions can lead to different age determinations, and we emphasize the importance of carefully selecting slit positions if one wishes (as we do) to find the major starburst regions. It is also far more difficult to obtain

a reliable age for an older population in the presence of a contaminating younger population than the reverse.

3.2. Interaction History

Images of Mrk 1014 show a very prominent tail extending to the northeast, reminiscent of the tidal tail of 3C 48 (CS2000). Like the tidal tail in 3C 48, this tail has a number of small clumps (see *HST* image in Fig. 3) of star formation, which are commonly found in merging systems. The bulk of the bright portion of the tail appears to be dominated by an intermediate age population (∼1 Gyr) with a very small contribution, if any, from an old underlying population; alternatively, it could be dominated by an older population, with some flux scattered from the bright star-forming regions (*a* through *d*) or fainter small regions distributed along the host. However, the north edge of the tail appears as a very sharp feature in the short wavelength images, and contains stellar populations which are as young as those of the clumps. As we find no redshift variations along this edge, it would appear that we are observing the tail nearly face-on, and that this is the leading edge where the material has been compressed, thus producing star formation. This, again, is similar to the blue leading edge observed in 3C 48 (Fig. 2*e* in CS2000), presumably sharper in Mrk 1014 because of the lower inclination angle.

Both the ground-based and the *HST* images of Mrk 1014 (Figs. 2 and 3) show a long, low-surface-brightness extension of the bright tail on the east of the nucleus and arching towards the south (more evident after the removal of the background galaxy, *k*) as well a very extended faint secondary tail, rotationally symmetric to the bright (primary) tail. Each tail extends for as much as $\sim 40''$ or ∼100 kpc (note the inset in Fig. 2 showing the well-known local interacting system M 51/NGC 5195 at the same scale). Spectra of the secondary tail west of the nucleus indicates that the tail is made up by older stars, and this is consistent with this tail being visible in our *H* (not shown) and K' images. No bright clumps of star formation are evident along the secondary tail; this absence is not unusual as tidal dwarf formation appears not to be a ubiquitous process in mergers (Hibbard & Yun 1999). The *HST* image of the nucleus (see inset in Fig. 3) shows a small extension on the south side which follows the direction of the secondary tidal tail. A similar extension is seen in *HST NICMOS* images by Scoville et al. (2000). There appears to be a "bulge" or enhanced brightness area elongated roughly along the axis connecting the beginning of both tails (*i.e.,* NW–SE), with a half radius of ~ 4 kpc. Assuming a projected velocity of 300 km s^{-1} on the plane of the sky, the dynamical age for the tails is ~ 330 Myr. The tails are then older than every major post-starburst knot they contain, consistent with the idea that the latter were formed after the tails were first launched. At the same time, the tails are dynamically younger than the bulk of the stars that form them, though perhaps only slightly so if the stellar populations observed in *f* and *g* are truly ~ 1 Gyr old, instead of being ~ 10 Gyr with a small admixture of younger stars.

Mrk 1014 shows some striking similarities to 3C 48 (CS2000): the morphology of the (primary) tidal tail, the clumps of star formation along the tail as well as its blue leading edge, the relation of

the starburst ages to the dynamical age of the tails (both ages ~ 200 Myr younger in 3C 48), and the clumpy extended emission line region (Stockton & MacKenty 1987) with high velocity (> 1000 km s^{-1}) components. As with 3C 48, the data strongly suggest that Mrk 1014 is the result of a merger of two galaxies of comparable size, both of which were disks in this case. The starbursts in the main body of the host of Mrk 1014, however, appear to be less intense and less widespread than those of 3C 48.

If the intermediate age (1 Gyr) population we see in regions f and g is real, it may be the relic of a starburst ignited at an initial passage of the two interacting galaxies. Indeed, we know of another system (UN J1025−0040; Canalizo et al. 2000) where the interacting galaxies have a difference in starburst ages of this order, possibly coincident with their orbital period. If this were the case for Mrk 1014, one might expect most of the star formation at the present to be very strongly concentrated towards the nucleus, as most of the gas would have been driven towards the center starting ~ 1 Gyr ago.

4. IRAS 07598+6508

The luminous, $z = 0.148$, radio-quiet QSO IRAS 07598+6508 was first detected by *IRAS*, identified as an AGN candidate by de Grijp et al. (1987), and spectroscopically identified as a QSO by Low et al. (1988). The optical spectrum of the QSO is dominated by extremely strong Fe II emission (Lawrence 1988; Lípari 1994), and the UV spectrum shows low- and high-ionization broad absorption lines (BAL) extending to blueshifts of 5200 to 22000 km s−1 (Hines & Wills 1995; Boroson & Meyers 1992).

Figures 7 and 8 show, respectively, ground-based and *HST* images of IRAS 07598+6508 (see Boyce 1996, for a PSF-subtracted version of the *HST* image). These images show two clumpy regions $\sim 7''$ south and southeast of the QSO, bright in the PSF subtracted U' image, but barely visible in H-band images (not shown). The great number of knots in these regions, presumably OB associations, already argues for recent star formation.

Our slit positions cover these two regions, labeled a and c in Fig. 9, as well as some of the fainter emission surrounding the nucleus. Spectra of these regions are shown in Fig. 10. Regions a and c are fit by single starburst models of ages 70 ± 15 and 32 ± 7 Myr respectively. The light from these starbursts dominates the spectra as we do not find any significant contribution from an older component. Although single burst models fit the data better than two-component models, there are still some discrepancies in the fit. The observed spectra show an excess with respect to the model in the region between 3900 Å and 4100 Å , apparently because the observed continuum is steeper in this region. To test whether the discrepancy could be an indication of scattered QSO light, we subtracted QSO spectra with several different scalings from the stellar spectra, but we were unable to obtain better fits.

In contrast to a and c, the spectra of the regions closer to the nucleus (labeled d and e in

Fig. 9) show an older stellar population (Fig. 10, bottom panel). The SEDs of these spectra are much redder and there is a clear, though not very prominent, 4000 Å break. We detect this old population from $\sim 2''$ to $\sim 8''$ north of the QSO and from $\sim 2''$ to $\sim 4\farcs5$ south of the QSO.

We were unsuccessful in attempting to subtract the QSO scattered light closer to the nucleus because of the strong light scattering along the slit in these regions. Therefore we are unable to determine whether the populations closest to the nucleus are as old as those of d and e or if there might be a younger starburst concentrated around the nucleus.

Regions a and c have a slightly higher redshift than the fainter emission around the QSO: $z_a = 0.1490 \pm 0.0001$ and $z_c = 0.1488 \pm 0.0001$, compared to $z_{d,e} = 0.1485 \pm 0.0002$ for the regions closer to the nucleus, but the difference is barely significant. Measuring a precise redshift for the QSO is difficult because of the strong Fe II emission contaminating the broad emission lines, and the absence of narrow emission lines. Values in the literature include $z_{\rm QSO} = 0.1488$ as measured from CO (Solomon et al. 1997) and $z_{\rm QSO} = 0.1483$ as measured from broad Balmer emission lines (Lawrence 1988); both are within 180 km s^{-1} (and within the errors) of the values we measure for the host galaxy.

IRAS 07598+6508 has some limited extended narrow emission as seen in the [O III] image in Fig. 7. The ionized gas seems to be correlated with the stellar component: the velocity difference between emission and absorption lines in regions where both are present is never larger than 50 km s^{-1} (notice the profile of Hβ in Fig. 10; emission is visible slightly redshifted with respect to the absorption).

Region b shows the strongest emission and appears brightest in the [O III] image. The emission line spectrum has an underlying blue continuum with stellar features. The 2-dimensional spectrum shows that this region is broken up into two discrete clumps a little over $1''$ each, having some small scale velocity structure. The line flux ratios indicate that the south clump has lower ionization, and it may be an H II region rather than gas ionized by the QSO. A second, fainter component with a velocity gradient from 0 to ~ 500 km s^{-1} apparently originating from the north clump extends $1''$ towards the south.

About $11''$ north of the QSO, we find another emission region (labeled g) which is visible in the [O III] image, but not in any of the broad band images. No stellar continuum is evident from the spectrum, either. This region is also broken into two discrete, somewhat larger clumps, but in this case the clump closer to the nucleus has lower ionization. Both clumps are at a lower redshift than those of region b, *i.e.,* $z_{\rm em} = 0.1483 \pm 0.0001$ *vs.* $z_{\rm em} = 0.1491 \pm 0.0001$ in b.

Our deep R' image (Fig. 7) shows a tidal tail extending from north to the east and arching towards the south of the nucleus for $\sim 22''$ or ~ 50 kpc. The dynamical age of this feature (assuming a projected velocity of 300 km s^{-1}) is ~ 160 Myr, again older than the starbursts ages found for this object. We have a very faint spectrum of this tail at region f. The SED of the spectrum is similar to that of d and e, but the spectrum is too noisy to show stellar features. An [O II] λ3727 emission line is confined to this region (as seen in the 2-d spectrum) at a redshift of $z_{\rm em} = 0.1487$,

which is probably close to that of the stellar component as in other regions.

This tidal tail is strongly suggestive of a merger. The fact that only one tail is evident may indicate that we are seeing the result of a merger of a spiral with an elliptical galaxy. This configuration, however, could also result from the merger of two spiral galaxies, one of which is counter rotating to the relative orbit. In mergers with such geometry, the gas and stars in the counter-rotating disk are only slightly perturbed and are not pulled into tidal bridges and tails (Toomre & Toomre 1972; Hibbard & Yun 1999). It is also possible that a second tail may not be evident because of projection effects.

Regions *a* and *c* may be part of the host galaxy with enhanced surface brightness due to the recent star formation, or they may be remnants of companion galaxies which have strongly interacted with the host galaxy. In either case it is clear that these regions are tidally disturbed and they will likely be completely mixed with the host within a few crossing times.

The two galaxies $\sim 14''$ south of the QSO are likely to be companion galaxies since they are bright in our [O III] image (Fig. 7), but we do not have a spectrum to confirm this. The colors for the SE galaxy indicate that it may have recent star formation, if at the same redshift as IRAS 07598+6508. We find two additional objects with the same redshift as IRAS 07598+6508 that happened to fall in our slits: a faint emission line object $\sim 20''$ south-southwest of the QSO, and a bright galaxy with an absorption and emission line spectrum $\sim 60''$ southwest of the QSO.

5. Mrk 231

Mrk 231 ($z = 0.042$), often classified as a Seyfert 1 galaxy, is slightly below the luminosity cutoff for QSOs defined by Schmidt & Green (1983). However, the nucleus is heavily reddened, with an estimated $A_V \approx 2$ of foreground extinction (Boksenberg et al. 1977; Lípari 1994; see also Goodrich & Miller 1994), so it would be well above this threshold if it were unobscured. The central plateau of the host galaxy is off center with respect to the nucleus, and the presence of tails to the north and south, as well as a low-surface-brightness extension to the east clearly indicate a recent merger (Fig. 11). Closer to the nucleus, *HST* imaging shows a large number of stellar associations indicating recent star formation (Surace et al. 1998; see Fig. 12).

As in the case of IRAS 07598+651, the spectrum of the QSO is dominated by strong Fe II emission (Lípari et al. 1994) and shows a peculiar low-ionization BAL system with velocities up to -7800 km s^{-1} (Smith et al. 1995; Foster et al. 1995). Previous spectroscopy of the host galaxy indicates the presence of a young stellar population (Hamilton & Keel 1987).

We have obtained and modeled spectra of several regions in the host galaxy as labeled in Fig. 13. In regions *k* and *i*, we find no evidence for a significant young starburst population. A 10 Gyr-old population with an exponentially decreasing SFR and an e-folding time of 5 Gyr fits this spectrum quite well, as shown in the bottom panel of Fig. 14. Therefore we use this model as an

underlying population to fit the rest of the spectra in the host galaxy.

Unfortunately, because of the poor sensitivity of LRIS shortwards of 4000 Å, and the fact that Mrk 231 has a lower redshift ($z = 0.042$) than the other two objects, we were unable to obtain the near-UV portion of the spectrum, which is the most helpful region in determining the ages of post-starburst populations. We are left then with the region on the long side of 3800 Å, where more than one combination of models can give similar fits to the spectra.

Indeed, we found degenerate fits in some regions of the host galaxy, particularly in those regions with the youngest populations and those where the absorption lines were heavily contaminated by emission so that we could not use Balmer lines to discriminate between models. In such regions we obtained two χ^2 minima, generally with one corresponding to a model with a small contribution (*i.e.,* small percentage of total mass along the line of sight) from a very young starburst, and the other to a model with a large contribution from a somewhat older starburst. We illustrate the problem in Fig. 15, where we have plotted two models resulting from a 4 Myr and a 42 Myr old populations contributing, respectively, 1% and 12% of the total luminous mass. The models are nearly identical in the spectral region redwards of 3800 Å, and both are good fits to the data (see inset in Fig. 15) with χ^2 values for these models differing only by 10%. The models, however, diverge quickly at shorter wavelengths.

In order to discriminate between the two "best fits" to the data, we have measured photometry of the different regions (*a* through *k* as indicated in Fig. 13) from our ground-based optical images. We have been careful to measure fluxes only within the areas limited by the slits, at similar resolutions, and subtracting scattered light from the QSO where necessary. The solid circles in Fig. 15 indicate the photometry of region *a*. Clearly, the older model (red line) is a better fit to the data. It is important to note, however, that if there is considerable reddening by dust along the lines of sight to these regions in the host galaxy, the flux values of U' will be depressed; therefore the photometric points can only help us to determine upper limits to the ages of the stellar populations. For consistency, the age errors quoted in this section are as defined in §2.1, and do not take into account additional constraints placed by the photometry.

Region *a* corresponds to the west side of the arc-shaped structure (the "horseshoe"; Hamilton & Keel 1987), $\sim 4''$ south of the QSO nucleus. The *HST* F702W image in Fig. 12 shows that region *a* is formed by multiple knots, much like those of regions *a* and *c* in IRAS 07598+6508. However this structure, unlike those of IRAS 07598+6508, has a remarkably similar morphology from the near UV to the near IR as shown in the top right panel of Fig. 11. As discussed above, we determine an age of 42 (+22, -17) Myr. This age is younger than the 225 Myr estimated from $U-B$ colors of this region by Surace & Sanders (2000).

While several authors have noted the blue color of the "horseshoe" (*e.g.,* Kodaira et al. 1979; Hutchings & Neff 1987), we find a region that is relatively much brighter at shorter wavelengths $16''$ south of the QSO, labeled *c* in Fig. 13. This region appears as a bright blue extended blob dominating the $U'-B$ color map in Fig. 11. The spectrum has a very steep blue continuum, and

very strong emission lines at the same redshift as the absorption lines, likely from an H II region (Hamilton & Keel 1987). The top panel of Fig. 14 shows the spectrum of region c with the Balmer emission lines subtracted as described in §2.1. We find an age for this region of 5 Myr. As such a young starburst age is comparable to the expected duration of a typical individual starburst, and we are likely observing a collection of several such starbursts, it is virtually impossible to distinguish between continuous star formation and instantaneous bursts. The age we find is, therefore, simply indicative of ongoing star formation. As in region a, we find degeneracy in the modeling of this spectrum, with a second χ^2 minimum at 100 Myr. The near-UV continuum of the older model, however, falls 2σ below the U' photometric point. Neither the deep optical ground-based images nor the *HST* image show evidence for stellar associations in region c. This is somewhat surprising since, although the starburst population contributes only 1% to the luminous mass along the line of sight, its flux amounts to 42% of the total flux at 5000 Å(rest wavelength), and even more at shorter wavelengths.

Regions b and e appear as single clumps in the images and have ages of 140 (+80, −70) Myr and 180 (+60, −80) Myr respectively. The starburst populations dominate the spectra in these regions, contributing $\sim 75\%$ of the total flux at rest frame 5000 Å and up to 36% of the total luminous mass along the line of sight. Regions d, f (Fig. 14), g, and h all show very similar spectra, as expected from the color maps (Fig. 11), with ages between 300 and 360 Myr. The starbursts in these regions typically contribute only ∼50% to the total flux and $\sim 15\%$ of the total luminous mass, except for region d, for which these values are very similar to those of regions b and e.

We detect very weak continuum from the north tail (region l) at the 2.5σ level. The continuum is slightly blue, and there is a hint of Mg Ib at the redshift of the host galaxy. This region corresponds to the blue region in the $B-V$ color map, just before the condensation at the end of the north tail. It is possible that this region contains a knot of star formation like those found in the tail of Mrk 1014.

Lípari (1994) reports the presence of an extended Na I D BAL in the west side of the host galaxy. The only place where we see evidence for this feature is in region j. The spectrum of j, uncorrected for QSO scattered light, shows a wide absorption feature ($\sim$ 1900 km s^{-1} FWHM compared to $\sim$ 1050 km s^{-1} for the QSO Na I D BAL) as well as narrow absorption and emission (see below) at the redshift of the stellar component. After correcting for QSO contamination, the feature appears narrower, but still at ~ -6400 km s^{-1} with respect to the emission line. The hypothetical BAL feature is, however, much weaker than that of the QSO, and it could be an artifact of an imperfect subtraction of the QSO light.

While the evidence for extended BAL is not strong in our data, Hamilton & Keel (1987) find an "excess flux" extending to the blue side of [N II] λ6548, which they interpret as a broad blueshifted component of Hα or Hα + [N II] indicative of an outflow with velocities up to 1500 km s^{-1}. We observe this excess most clearly in regions h and g extending to even larger velocities (~ -2500 km s^{-1}). Boroson & Meyers (1992) find some level of excess light in the blue wing of the Hα line

in every low-ionization BAL QSO in their sample and suggest that this excess flux could be from the BAL material itself.

The narrow Na I *D* emission line shows a peculiar behavior. We observe narrow Na I *D* emission in regions *h* and *j* on the red side of the absorption line, forming what looks like a P-cygni profile. The only other emission lines evident in region *h* are [N II] λ6583, and weak [S II] $\lambda\lambda$6717,6731, but these lines are slightly *blueshifted* with respect to the absorption lines. In region *g* the Na I *D* emission line disappears, but the absorption line becomes very weak as well, so it is possible that the emission line is blueshifted into the absorption line; [N II], however, is at a higher redshift than in region *h*. Thus, the very low ionization gas appears to be decoupled from the moderately low ionization gas in these regions.

Hutchings & Neff (1987) find a "green" (*i.e.,* visible only in their $G-B$ image), jet-like feature extending from near the nucleus to the northeast. They suggest it "may be line emission in [O III], perhaps tracing ionizing radiation originating in the nucleus". Our slit goes through the western side of where this feature would be (see Fig. 2 in Hutchings & Neff 1987), and region *j* should sample the brightest part of the ridge leading to the bright knot. However, we find only weak [O III] in the spectrum of this region, certainly much weaker than in other regions we sample. Therefore it is unlikely that this "green" feature, if real, is due to ionized gas.

Images of Mrk 231 show a greatly disturbed host galaxy both in large and small scales (Fig. 11). At large scales, two symmetric tails extend on the east side of the nucleus for $\sim 44''$ or ~ 35 kpc each, and there is some very extended low surface brightness material east of the north tail. The nucleus is off-center on a bright "plateau" (Hamilton & Keel 1987) 20 kpc across that shows complex morphology, including linear jet-like structures (region *g*), and curved tail-like structures (region *d*). Closer to the nucleus (Fig. 12) we find the "horseshoe" 3 kpc to the south with numerous clumps of star formation, and arm-like features spiraling around the nucleus which connect to the outer tidal tails (Surace et al. 1998) This morphology is indicative of a merger between two disk galaxies of similar mass.

While we are unable to obtain stellar spectra within the central kpc ($< 2''$) of Mrk 231, Smith et al. (1995) have found from UV spectropolarimetry of the nuclear region that high polarization in the optical falls off quite rapidly shortward of ~ 3000 Å; this effect is most easily interpreted as a dilution of the polarized component by O and B stars from an ongoing starburst (Smith et al. 1995). CO and radio observations also show evidence for a centrally concentrated starburst (Downes & Solomon 1998; Taylor et al. 1999). It is possible that the knots along the arm-like features around the nucleus have ages similar to those of region *a*, if not younger.

We find a relatively wide range of starburst ages around the host galaxy. If, once again, we assume a projected velocity of 300 km s^{-1}, the tidal tails have a dynamical age of 110 Myr. Mrk 231 is unusual in that there seems to be a significant post-starburst population somewhat older (300–360 Myr) than the tails, which may indicate that wide spread star formation was ignited prior to the stages of final merger. Numerical simulations of mergers (Mihos & Hernquist 1996) predict

such a scenario when the merging galaxies lack a significant bulge to stabilize them against an early dissipation. In CS2000 we noted that the apparent correlation between bulge mass and black-hole mass (Magorrian et al. 1998) suggests a possible correlation between QSO luminosity and the delay in star formation activity. Thus, the early starburst activity in Mrk 231 may indicate that the host galaxy did not have a substantial bulge, which would in turn imply a less massive black-hole that may result into a less luminous AGN. Although we do in fact observe a relatively less luminous AGN in Mrk 231, these connections are highly speculative, and they are based on relations (Magorrian et al. 1998) and models (Mihos & Hernquist 1996) that still have many uncertainties.

6. Discussion

Mrk 1014, IRAS 07598+6508, and Mrk 231 show many similarities. We already knew that these three objects, while being optically or IR selected QSOs, were also part of the ULIG family. In this study we have found additional properties which they share and which may be related to their intermediate position in the FIR diagram.

While Mrk 1014 and Mrk 231 have long been known to have tails, we have shown that IRAS 07598+6508 also has at least one tidal tail. We have found evidence that all three objects have undergone a strong interaction and are now in the final stages of mergers. The morphology of the hosts (highly perturbed galaxies with tidal tails and destroyed disks) as well as the extent of the starbursts indicate that these are all major mergers between galaxies of comparable mass rather than accretion events of low mass dwarf companions (Mihos & Herquist 1994; Mihos & Hernquist 1996).

All three objects show spectra typical of E+A galaxies (Dressler & Gunn 1983), that is, spectra characterized by the simultaneous presence of strong Balmer absorption lines indicative of a young stellar population and features from an older population such as Mg I*b*, and the absence of strong emission lines typical of star forming galaxies (we reiterate that the emission lines seen in our spectra generally come from extended gas ionized by the QSO rather than from star forming regions, with a few exceptions). E+A galaxies are frequently linked to galaxy-galaxy mergers and interactions (*e.g.,* Zabludoff 1996). In the case of objects with E+A spectra undergoing tidal interactions, the young superposed population is clearly related to the interaction. The three objects discussed in this paper, along with 3C 48 (CS2000) and PG 1700+518 (CS97), all have interaction-induced starbursts.

In addition to the similarities noted in the host galaxies of the three objects, there are also some common characteristics in the spectra of the active nuclei themselves. All three objects show strong Fe II emission, with two of these objects (IRAS 07598+6508 and Mrk 231) being "extreme" Fe II emitters (*i.e.,* showing ratios of $I(\mathrm{Fe\,II}\ \lambda4570)/I(\mathrm{H}\beta) > 2$; Lípari 1994). The latter two objects, like PG 1700+518 (CS97; SCC98), are also low-ionization BAL QSOs and have weak or absent narrow emission lines.

How do the ages of these starbursts relate to the merger/interaction stage? The dynamical ages for tidal features in these objects are uncertain because of projection effects. However, our rough estimates indicate that in two cases, Mrk 1014 and IRAS 07598+6508, the peak of the starburst occurred after the tidal tails were launched. This requires some mechanism to stabilize the gas contents of the galaxies against bursting in star formation until the later stages of the merger; numerical simulations indicate that a significant bulge in the host can provide this mechanism (Mihos & Hernquist 1996). Mrk 231, on the other hand, shows starburst ages which indicate that much of the star formation activity may have started before the last stages of the merger; hence, one or both of the merging galaxies may have lacked a significant bulge.

Whenever we have found a significant range of starburst ages in the host galaxies of QSOs, we have also found evidence that the youngest major starburst regions are preferentially concentrated towards the center of the galaxy. In 3C 48 (CS2000) we found the clearest example of this, with starburst ages becoming progressively younger and more dominating as we approached the galaxy/QSO nucleus. Mrk 231 shows older starbursts in the "plateau" extending ~ 12 kpc around the nucleus, with some of the youngest populations only 3 kpc from the nucleus, and possibly even younger populations in the central kpc of the galaxy. Mrk 1014 shows stronger relatively recent star formation activity along the tail than any of the other objects. However, the starburst region we observe within 2 kpc of the nucleus is far more massive, luminous, and larger (Surace et al. 1998) than the starburst regions along the tail, and has the youngest age found in the host.

The interaction histories of the five objects discussed so far clearly favor a strong connection between interactions and vigorous bursts of star formation. Since the gas flows towards the inner regions can not only trigger star formation but also serve as fuel to the QSO, one might expect the age of the QSO activity to be closely related to the age of the initial starbursts in the central regions of the galaxy. However, observations of central starbursts are in every case hampered by the presence of the QSO; even if this region could be observed, the spectrum would likely be dominated by continuing recent starburst activity and not by a starburst that was coincident with the onset of the QSO activity. Furthermore, both starburst and QSO activity may be episodic. All of this is to say that there is an unavoidable intrinsic uncertainty in using starburst ages to place QSOs in an evolutionary sequence. We defer the detailed discussion of a possible age sequence to a subsequent paper where we will present the results of the four remaining objects in our sample (*i.e.,* IRAS 00275−2859, IRAS 04505−2958, I Zw 1, and PG 1543+489).

We emphasize, though, that many of our general conclusions from the objects discussed here, as well as from our observations of 3C 48 (CS2000), have an interest that is quite independent of any attempt to use some sort of starburst age as a proxy for a QSO age. (1) The confirmation that these are all starburst or post-starburst objects and that they all show obvious tidal tails validates their close connection with other ULIGs, virtually all of which are mergers or strongly interacting pairs. While there has long been strong *circumstantial* evidence that a large fraction of the QSO population has resulted from triggering of the QSO activity by interactions and mergers, we now have much more direct evidence for this mechanism for at least one subclass of QSOs. (2) Both the spatial

distribution and the time history of star formation in a QSO host galaxy give clues to nature of the galaxies that have participated in the merger. While more sophisticated models of star formation during interactions will be necessary to exploit these data fully, we already have some hints in terms of the enhanced star formation along the leading edge of the tails in 3C 48 and Mrk 1014, and in the relative ages of the tail structures and the star-forming regions contained within them. (3) The youth of the stellar populations in these objects reinforces previous suggestions connecting strong Fe II emission and low-ionization BAL features with the relatively recent triggering of QSO activity. We will discuss these connections in detail in the paper presenting the observations of the remaining four objects in our sample.

We thank Gerbs Bauer, Scott Dahm, and Susan Ridgway for assisting in some of the observations, and Bill Vacca for helpful discussions about IMFs. We also thank the referee, Dean Hines, for his very prompt review of the paper and his suggestions, which helped us improve both its content and its presentation. This paper was partly written while both authors were visitors at the Research School of Astronomy and Astrophysics of the Australian National University, and we thank both the Director, Jeremy Mould, and the staff there for their hospitality. This research has made use of the NASA/IPAC Extragalactic Database (NED) which is operated by the Jet Propulsion Laboratory, California Institute of Technology, under contract with the National Aeronautics and Space Administration. This research was partially supported by NSF under grant AST95-29078.

REFERENCES

Andreani, P., Franceschini, A., & Granato, G. 1999, MNRAS, 306, 161

Boksenberg, A., Carswell, R. F., Allen, D. A., Fosbury, R. A. E., Penston, M. V., & Sargent, W. L. W. 1977, MNRAS, 178, 451

Boroson, T. A., & Meyers, K. A. 1992, ApJ, 397, 442

Boyce, P. J. et al. 1996, ApJ, 473, 760

Bruzual A., G. & Charlot, S. 1996, unpublished [ftp://gemini.tuc.noao.edu/pub/charlot/bc96]

Bryant, P. & Scoville, N. Z. 1996, ApJ, 457, 678

Canalizo, G., Stockton, A., Brotherton, M. S., & van Breugel, W. 2000, AJ, 119, 59

Canalizo, G., & Stockton, A. 2000, ApJ, 528, 201 [CS2000]

Canalizo, G., & Stockton, A. 1997, ApJ, 480, L5 [CS97]

Clements, D. L. et al. 1996, MNRAS, 279, 459

de Grijp, M. H. K., Miley, G. K., & Lub, J. 1987, A&AS, 1987, 70, 95

Downes, D., & Solomon, P. M. 1998, ApJ, 507, 615

Dressler, A. & Gunn, J. E. 1983, ApJ, 270, 7

Foster, K., Rich, R. M., & McCarthy, J. K. 1995, ApJ, 450, 74

Goodrich, R. W. & Miller, J. S. 1994, ApJ, 434, 82

Gunn, J. E. 1979 in *Active Galactic Nuclei*, ed. C. Hazard and S. Mitton (New York: Cambridge University Press), p. 213

Hamilton, D. & Keel, W. C. 1987, ApJ, 321, 211

Heckman, T. M., Bothun, G. D., Balick, B., & Smith, E. P. 1984, AJ, 89, 958

Hibbard, J. E. & Yun, M. S. 1999, AJ, 118, 162

Hines, D. C., Low, F. J., Thompson, R. J., Weymann, R. J., & Storrie-Lombardi, L. 1999, ApJ, 512, 140

Hines, D. C. & Wills, B. J. 1995, ApJ, 448, 69

Hughes, D. H., Kukula, M. J., Dunlop, J. S., Boroson, T. 2000, MNRAS, in press [astro-ph/0002021]

Hutchings, J. B., & Crampton, D. 1990, AJ, 99, 37

Hutchings, J. B., & Neff, S. G. 1987, AJ, 92, 14

Hutchings, J. B., & Neff, S. G. 1992, AJ, 104, 1

Kodaira, K., Iye, M., & Nishimura, S. 1979, PASJ, 31, 451

Lawrence, A. et al. 1988, MNRAS, 235, 261

Lípari, S. 1994 ApJ, 436, 102

Lípari, S., Colina L., & Macchetto F., 1994 ApJ, 427, 174

Low, F. J., Huchra, J. P., Kleinmann, S. G., Cutri, R. M. 1988, ApJ, 327, L41

MacKenty, J. W., & Stockton, A. N. 1984, ApJ, 283, 64

McLeod, K. K., & Rieke, G. H. 1994, ApJ, 431, 137

Magorrian, J., et al. 1998, AJ, 115, 2285

Massey P., Strobel K., Barnes, J. V., & Anderson, E. 1988, ApJ, 328, 315

Mihos, J. C., & Hernquist L. 1996, ApJ, 464, 641

Mihos, J. C., & Hernquist L. 1994, ApJ, 425, L13

Neugebauer, G., Soifer, B. T., & Miley, G. K. 1985, ApJ, 295, L27

Neugebauer, G., Miley, G. K., Soifer, B. T., & Clegg, P. E. 1986, ApJ, 308, 815

Nolan, L. A., Dunlop, J. S., Kukula, M. J., Hughes, D. H., Boroson, T., Jimenez, R. 2000, MNRAS, in press [astro-ph/0004325]

Oke, J. B., et al. 1995, PASP, 107, 375

Sanders, D. B., Soifer, B. T., Elias, J. H., Madore, B. F., Matthews, K., Neugebauer, G., & Scoville, N. Z. 1988, ApJ, 325, 74

Sanders, D. B., Scoville, N. Z., & Soifer, B. T. 1988, ApJ, 335, 1

Scalo, J. M. 1986, Fund. Cosmic Phys., 11, 1

Scoville, N. Z., Evans, A. S., Thompson, R., Rieke, M., Hines, D. C., Low, F. J., Dinshaw, N., Surace, J. A., Armus, L. 2000, AJ, 119, 991

Schlegel, D. J., Finkbeiner D. P., & Davis, M. 1998, ApJ, 500, 525

Schmidt, R., & Green, R. F. 1983, ApJ, 269, 352

Smith, P. S., Schmidt, G. D., Allen, R. G., & Angel, J. R. P. 1995, ApJ, 444, 146

Solomon P. M., Downes, D., Radford, S. J. E., & Barrett, J. W. 1997, ApJ, 478, 144

Stockton, A. 1999, in Galaxy Interactions at Low and High Redshift, IAU Symp. 186, eds. D. Sanders & J. Barnes (San Francisco: Astron. Soc. Pac.), p. 311

Stockton, A. 1982, ApJ, 257, 33

Stockton, A., Canalizo, G., & Close, L. 1998, ApJ, 500, L121 [SCC98]

Stockton, A., & MacKenty 1987, ApJ, 316, 584

Surace, J. A., Sanders, D. B., Vacca, W. D., Veilleux, S., & Mazzarella, J. M. 1998, ApJ, 492, 116

Surace, J. A. & Sanders, D. B. 2000, AJ, in press [astro-ph/0005122]

Taniguchi, T., Kawara, K., Nishida, M., Tamura, S., Nishida, M. T. 1988, ApJ, 95, 1378

Taylor, G. B., Silver, C. S., Ulvestad, J. S., & Carilli, C. L. 1999, ApJ, 519, 185

Toomre, A., & Toomre, J. 1972, ApJ, 178, 623

Veilleux, S. & Osterbrock, D. E. 1987, ApJS, 63, 295

Zabludoff, A. I. et al. 1996, ApJ, 466, 104

This preprint was prepared with the AAS LaTeX macros v5.0.

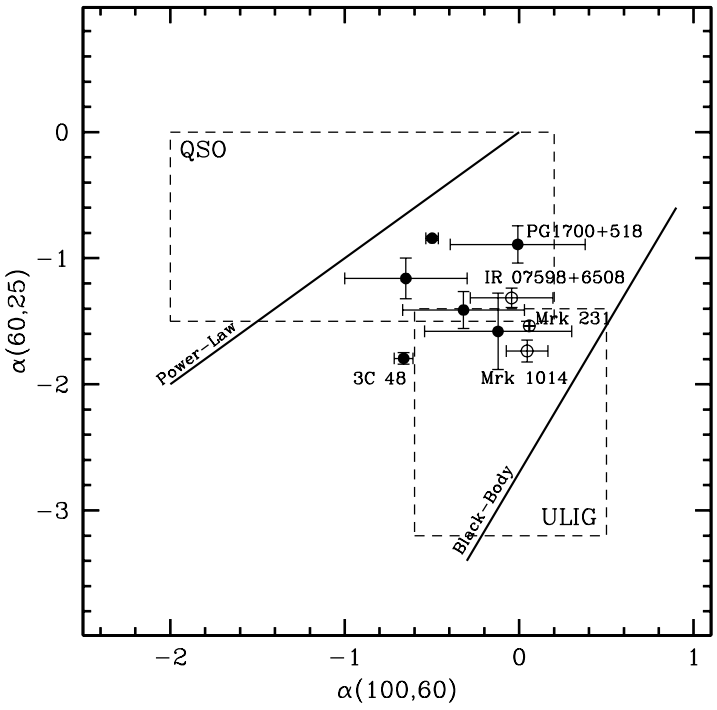

Fig. 1.— Far infrared spectral index plot (adapted from Lípari 1994). Different kinds of objects such as QSO/Seyferts and ultraluminous IR galaxies, occupy fairly well defined regions in the diagram (see, *e.g.,* Neugebauer et al. 1985). The objects in our sample have an intermediate position between these populations. The open circles show the positions of the three objects that are the subject of this paper.

Fig. 2.— Morphology and colors in the host galaxy of Mrk 1014. The main panel on the left shows a R'-band image, heavily smoothed to show the low-surface-brightness features; the upper-left inset shows the well known local interacting pair M51/NGC 5195, scaled to the distance of Mrk 1014, to indicate the size of the Mrk 1014 host galaxy. A lower-contrast version of the same Mrk 1014 image with less smoothing and with the PSF subtracted is shown at the middle top. K' and B'-band images are shown at the top right and bottom middle, respectively, and the $B'-R'$ color image is shown at the bottom right. The latter is coded so that regions with most negative $B'-R'$ show as blue, while relatively redder regions show as yellow and red. The region near the nucleus is dominated by the QSO and does not indicate the color of the host galaxy.

Fig. 3.— *HST* WFC2 image of Mrk 1014 obtained with the F675W filter. For this and the following *HST* images, the image has been rotated so that north is at the top and east to the left.

Fig. 4.— Slit positions and region identifications for Mrk 1014.

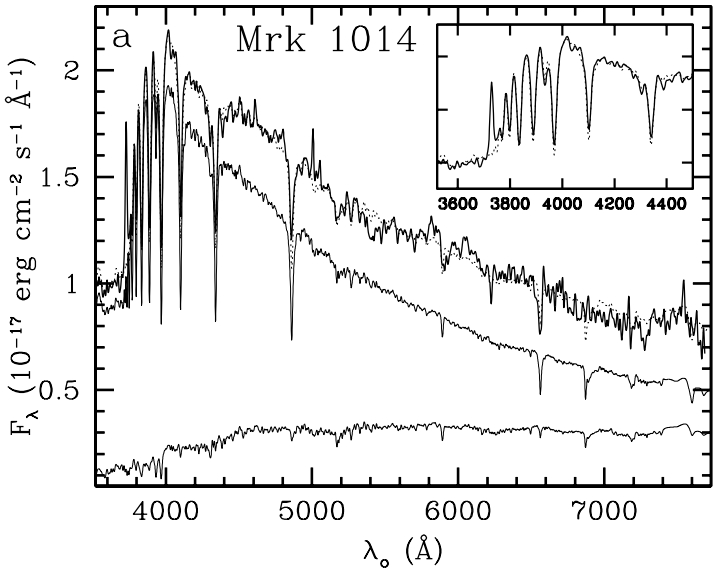

Fig. 5.— Rest frame spectrum of region *a* in the host galaxy of Mrk 1014 (heavy line), underlying old stellar population (lower light line), 200 Myr instantaneous starburst model (upper light line) and the χ^2 fit of the sum of the two models to the data (dotted line). The old model is a 10 Gyr old stellar population with an exponentially decreasing star formation rate with an e-folding time of 3 Gyr. The original data have been smoothed with Gaussian filters with $\sigma = 2$ Å. The inset shows in detail the blue part of the spectrum. In this and the following figure, emission lines come from the extended ionized gas around the QSO, and not from star forming regions. These lines have not been included in calculations of χ^2.

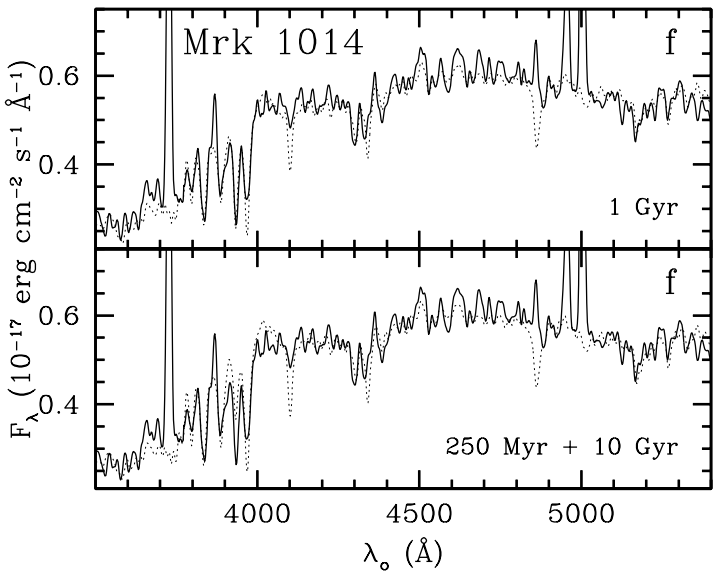

Fig. 6.— Rest frame spectrum of region f in the host galaxy of Mrk 1014 (solid line in both panels). The dotted line in the top panel is a single 1 Gyr instantaneous burst model. The dotted line in the bottom panel is the best χ^2 fit to the data of the sum of a 250 Myr instantaneous burst model and an old population (see text for details).

Fig. 7.— Morphology in the host galaxy of IRAS 07598+6508. The main panel on the left and the top two panels on the right show the R' image at a range of contrasts, while the lower panels on the right show the U' and [O III] images. All images have had the PSF removed, using the bright star to the north-west as the PSF template.

Fig. 8.— *HST* PC1 image of IRAS 07598+6508 obtained with the F702W filter.

Fig. 9.— Slit positions and region identifications for IRAS 07598+6508.

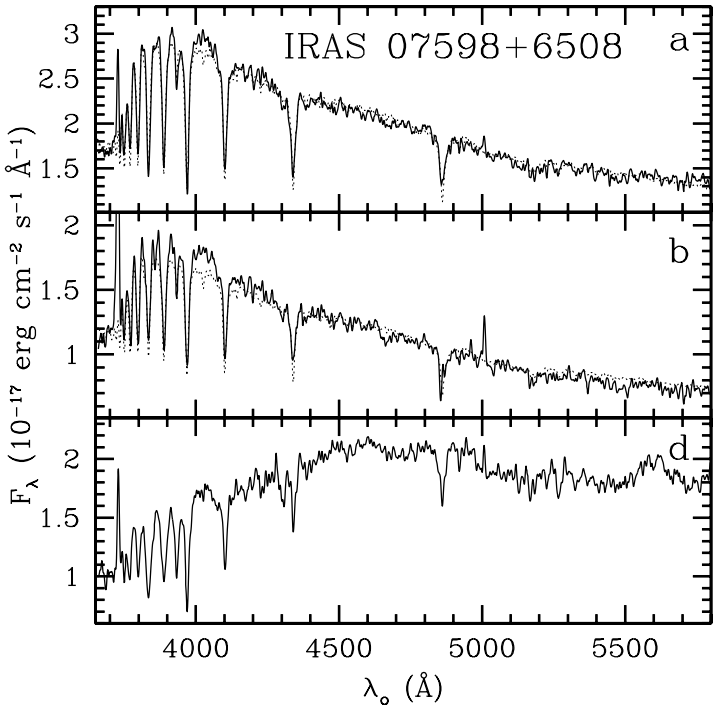

Fig. 10.— Rest frame spectra of regions *a*, *b*, and *e* (from top to bottom) in the host galaxy of IRAS 07598+6508. For panels *a* and *b*, the solid lines are the observed spectra and the dotted lines are instantaneous burst models of 70 and 30 Myr, respectively.

Fig. 11.— Morphology and colors in the host galaxy of Mrk 231. The main panel on the left and the top two panels on the right show the B-band image. The insert in the top-right panel shows an H-band image of the inner regions (note that the images in this panel are magnified by a factor of two compared with those in the other panels); the similarity in the structure seen in the arc-like region south of the nucleus indicates that the SEDs of the emission regions within this region are all similar and that reddening is not a severe problem. The two lower-right panels show $B-V$ and $U-B$ images, respectively; more negative values are indicated as blue. Note the relative colors of the arc and the patch about $16''$ south of the nucleus (essentially regions a and c in Fig. 4), indicating the much younger population in the latter.

Fig. 12.— *HST* PC1 image of the inner region of Mrk 231 obtained with the F439W filter.

Fig. 13.— Slit positions and region identifications for Mrk 231.

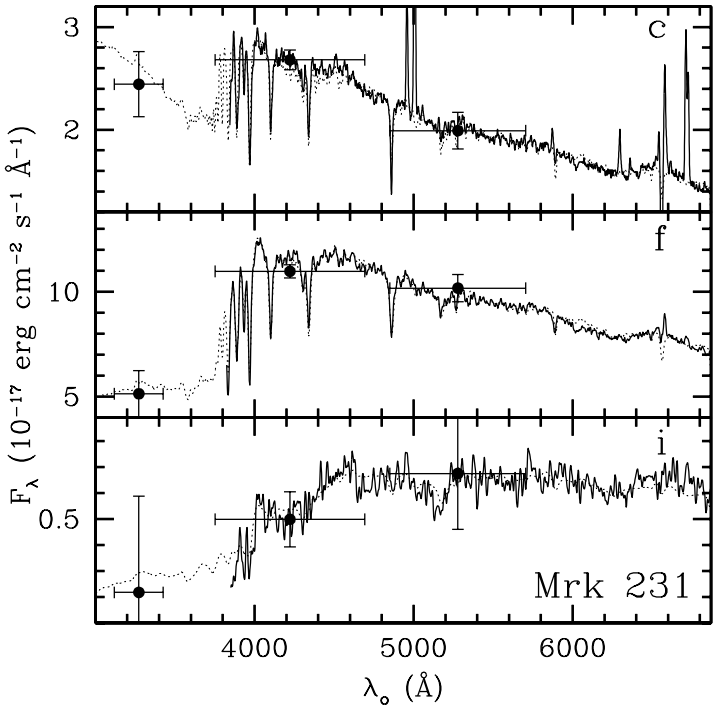

Fig. 14.— Rest frame spectra of regions c, f, and i (from top to bottom) in the host galaxy of Mrk 231. Each panel shows the observed spectrum (solid line), the best χ^2 fit of the model to the data (dotted line), and the photometry of the region from our U', B, and V images. The error bars in the horizontal direction represent the de-redshifted bandpasses, while those in the vertical direction are 1σ random uncertainty in the flux. Balmer emission lines of the spectrum in panel c have been subtracted, assuming case B recombination.

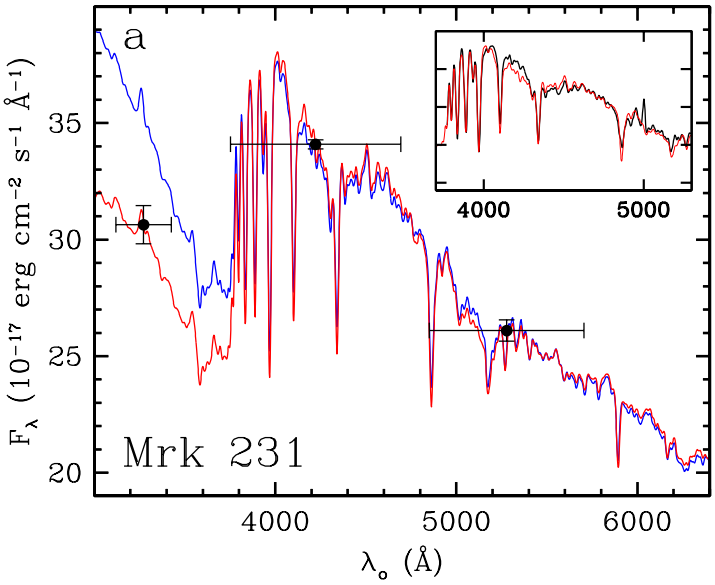

Fig. 15.— Degeneracy in the modeling of spectra in the host galaxy of Mrk 231. The main panel shows two spectral synthesis models giving very similar fits to the rest-frame spectrum of region *a* redwards of 3800 Å. The blue line is the sum of an old (10 Gyr with exponentially decaying SFR) model and a 4 Myr instantaneous burst model that contributes 1% of the luminous mass. The red line is the sum of the same old population and a 42 Myr instantaneous burst model that contributes 12% of the luminous mass. There is only a 10% difference in χ^2 of the fit of each of these models to the data. The inset shows the actual spectrum of region *a* with (black line) and the older of the two models.

Table 1. Journal of Spectroscopic Observations

Object	PA (deg)	Offset (arcsec)	Dispersion (Å pixel^{-1})	Total Int. Time (s)	UT Date
Mrk 1014	103.0	4.0 N	2.44	3600	97 Sep 13
Mrk 1014	87.1	6.9 N	2.44	3600	98 Sep 01
Mrk 1014	148.6	2.2 W	2.44	2400	98 Sep 01
IRAS 07598+6508	243.6	6.9 S	1.28	3600	96 Oct 13
IRAS 07598+6508	190.0	0.0	1.28	3600	96 Oct 14
Mrk 231	6.0	0.0	2.44	1800	97 Jun 12
Mrk 231	83.0	16.0 S	2.44	3600	98 Mar 21
Mrk 231	30.0	7.0 W	2.44	2400	98 Mar 21

Table 2. Journal of Imaging Observations

Object	Instrument	Filter[a]	Exposure (s)	Scale ($''$pix^{-1})	UT Date
Mrk 1014	Orbit CCD	U'	8×1200	0.138	97 Nov 01
Mrk 1014	Orbit CCD	B'	5×300	0.138	97 Oct 31
Mrk 1014	Tek1024 CCD	R'	5×300	0.222	91 Nov 13
Mrk 1014	QUIRC	H	29×300	0.061	99 Oct 29
Mrk 1014	NICMOS-3	K'	39×70	0.374	90 Oct 28
IRAS 07598+6508	Loral CCD	U'	8×1200	0.138	97 Mar 09
IRAS 07598+6508	Tek1024 CCD	R'	15×300	0.222	92 Mar 01
IRAS 07598+6508	Tek1024 CCD	[O III]	7×1560	0.222	92 Feb 27
IRAS 07598+6508	QUIRC	H	22×120	0.061	99 Oct 30
Mrk 231	Loral CCD	U'	5×1200	0.138	97 Mar 08
Mrk 231	Loral CCD	B	18×200	0.138	97 Mar 09
Mrk 231	Loral CCD	V	6×300	0.138	97 Mar 08
Mrk 231	QUIRC	H	69×20	0.061	99 Apr 04

[a]The U' filter was centered at 3410 Å with a bandpass of 320 Å. The B' filter used for Mrk 1014 had a smaller bandpass (593 Å) than the standard B filter to avoid strong emission lines. The R' filter used for Mrk 1014 was centered at 6815 Å with a bandpass of 1226 Å, and that used for IRAS 07598+6508 was centered at 6500 Å with a bandpass of 880 Å; both avoid strong emission lines. The [O III] filter was centered at 5777 Å with a bandpass of 100 Å.


This figure "canalizo.fig2.jpg" is available in "jpg" format from:
http://arXiv.org/ps/astro-ph/0007002


This figure "canalizo.fig3.jpg" is available in "jpg" format from:
http://arXiv.org/ps/astro-ph/0007002


This figure "canalizo.fig4.jpg" is available in "jpg" format from:
http://arXiv.org/ps/astro-ph/0007002


This figure "canalizo.fig7.jpg" is available in "jpg" format from:
http://arXiv.org/ps/astro-ph/0007002


This figure "canalizo.fig8.jpg" is available in "jpg" format from:
http://arXiv.org/ps/astro-ph/0007002


This figure "canalizo.fig9.jpg" is available in "jpg" format from:
http://arXiv.org/ps/astro-ph/0007002


This figure "canalizo.fig11.jpg" is available in "jpg" format from:
http://arXiv.org/ps/astro-ph/0007002


This figure "canalizo.fig12.jpg" is available in "jpg" format from:
http://arXiv.org/ps/astro-ph/0007002


This figure "canalizo.fig13.jpg" is available in "jpg" format from:
http://arXiv.org/ps/astro-ph/0007002